7 Electron–proton elastic scattering

In e^+e^- collisions, the initial-state particles are fundamental fermions. Consequently, the cross sections for processes such as e^+e^- annihilation are determined by the QED matrix element and the event kinematics (phase space) alone. Calculations of cross sections for collisions involving protons, for example at an electron–proton collider or a hadron collider, also need to account for the composite nature of the proton. This chapter describes low-energy electron–proton *elastic* scattering. The main purpose is to provide an introduction to a number of concepts which form the starting point for the description of the high-energy interactions of protons that is the main topic of the following chapter.

7.1 Probing the structure of the proton

Electron–proton scattering provides a powerful tool for probing the structure of the proton. At low energies, the dominant process is elastic scattering where the proton remains intact. Elastic scattering is described by the coherent interaction of a virtual photon with the proton as a whole, and thus provides a probe of the global properties of the proton, such as its charge radius. At high energies, the dominant process is deep inelastic scattering, where the proton breaks up. Here the underlying process is the *elastic* scattering of the electron from one of the quarks within the proton. Consequently, deep inelastic scattering provides a probe of the momentum distribution of the quarks.

The precise nature of the $e^-p \to e^-p$ scattering process depends on the wavelength of the virtual photon in comparison to the radius of the proton. Electron–proton scattering can be broadly categorised into the four classes of process shown schematically in Figure 7.1:

(a) at very low energies, where the electrons are non-relativistic and the wavelength of the virtual photon is large compared to the radius of the proton, $\lambda \gg r_p$, the $e^-p \to e^-p$ process can be described in terms of the elastic scattering of the electron in the static potential of an effectively point-like proton;

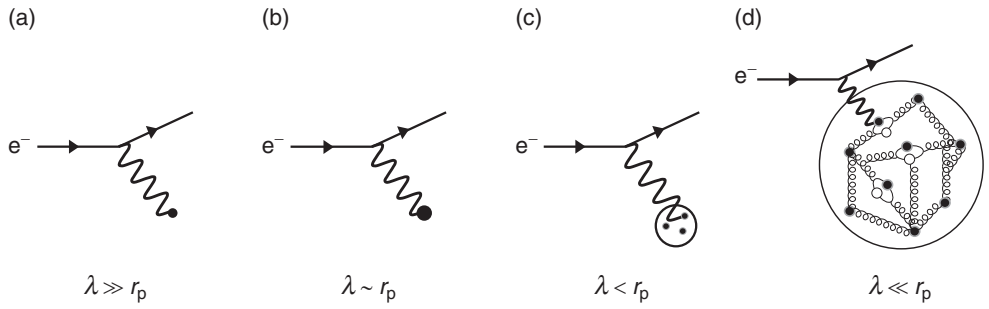

Fig. 7.1 The nature of e^-p scattering depending on the wavelength of the virtual photon.

(b) at higher electron energies, where $\lambda \sim r_p$, the scattering process is no longer purely electrostatic in nature and the cross section calculation also needs to account for the extended charge and magnetic moment distributions of the proton;

(c) when the wavelength of the virtual photon becomes relatively small, $\lambda < r_p$, the elastic scattering cross section also becomes small. In this case, the dominant process is inelastic scattering where the virtual photon interacts with a constituent quark inside the proton and the proton subsequently breaks up;

(d) at very high electron energies, where the wavelength of the virtual photon ($\lambda \ll r_p$) is sufficiently short to resolve the detailed dynamic structure of the proton, the proton appears to be a sea of strongly interacting quarks and gluons.

Whilst we will be interested primarily in the high-energy deep inelastic e^-p scattering, the low-energy e^-p elastic scattering process provides a valuable introduction to a number of important concepts.

7.2 Rutherford and Mott scattering

Rutherford and Mott scattering are the low-energy limits of e^-p elastic scattering. In both cases, the electron energy is sufficiently low that the kinetic energy of the recoiling proton is negligible compared to its rest mass. In this case, the proton can be taken to be a *fixed* source of a $1/r$ electrostatic potential. The cross sections for Rutherford and Mott scattering are usually derived from non-relativistic scattering theory using the first-order $\langle \psi_f | V(r) | \psi_i \rangle$ term in the perturbation expansion. Here the cross sections are derived using the helicity amplitude approach of the previous chapter, treating the proton as if it were a point-like Dirac particle. Provided the wavelength of the virtual photon is much larger than the radius of the proton, this is a reasonable approximation.

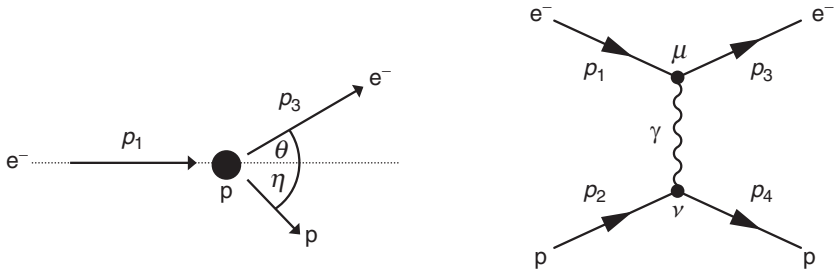

Fig. 7.2 Rutherford scattering of an electron from a proton at rest in the laboratory frame and the corresponding Feynman diagram.

In the limit where the proton is taken to be a point-like Dirac fermion, the matrix element for the Feynman diagram for low-energy e^-p elastic scattering, shown in Figure 7.2, is given by

$$\mathcal{M}_{fi} = \frac{Q_q e^2}{q^2} \left[\bar{u}(p_3)\gamma^\mu u(p_1)\right] g_{\mu\nu} \left[\bar{u}(p_4)\gamma^\nu u(p_2)\right]. \tag{7.1}$$

From (4.65), the Dirac spinors describing the two possible helicity states of the electron can be written in the form

$$u_\uparrow = N_e \begin{pmatrix} c \\ se^{i\phi} \\ \kappa c \\ \kappa s e^{i\phi} \end{pmatrix} \quad \text{and} \quad u_\downarrow = N_e \begin{pmatrix} -s \\ ce^{i\phi} \\ \kappa s \\ -\kappa c e^{i\phi} \end{pmatrix},$$

where $N_e = \sqrt{E + m_e}$, $s = \sin(\theta/2)$ and $c = \cos(\theta/2)$. The parameter κ is given by

$$\kappa = \frac{p}{E + m_e} \equiv \frac{\beta_e \gamma_e}{\gamma_e + 1},$$

where β_e and γ_e are respectively the speed and Lorentz factor of the electron. Writing the electron spinors in terms of the parameter κ clearly differentiates between the non-relativistic ($\kappa \ll 1$) and highly relativistic ($\kappa \approx 1$) limits. If the velocity of the scattered proton is small, its kinetic energy can be neglected, and to a good approximation the energy of the electron does not change in the scattering process. Hence the same value of κ applies to both the initial- and final-state electron. For an electron scattering angle θ (see Figure 7.2) and taking the azimuthal angle for the electrons to be $\phi = 0$, the possible initial- and final-state electron spinors are

$$u_\uparrow(p_1) = N_e \begin{pmatrix} 1 \\ 0 \\ \kappa \\ 0 \end{pmatrix}, \; u_\downarrow(p_1) = N_e \begin{pmatrix} 0 \\ 1 \\ 0 \\ -\kappa \end{pmatrix} \text{ and } u_\uparrow(p_3) = N_e \begin{pmatrix} c \\ s \\ \kappa c \\ \kappa s \end{pmatrix}, \; u_\downarrow(p_3) = N_e \begin{pmatrix} -s \\ c \\ \kappa s \\ -\kappa c \end{pmatrix}.$$

The electron currents for the four possible helicity combinations, calculated from (6.12)–(6.15), are

$$j_{e\uparrow\uparrow} = \bar{u}_\uparrow(p_3)\gamma^\mu u_\uparrow(p_1) = (E + m_e)\left[(\kappa^2 + 1)c, 2\kappa s, +2i\kappa s, 2\kappa c\right], \tag{7.2}$$

$$j_{e\downarrow\downarrow} = \bar{u}_\downarrow(p_3)\gamma^\mu u_\downarrow(p_1) = (E + m_e)\left[(\kappa^2 + 1)c, 2\kappa s, -2i\kappa s, 2\kappa c\right], \tag{7.3}$$

$$j_{e\downarrow\uparrow} = \bar{u}_\uparrow(p_3)\gamma^\mu u_\downarrow(p_1) = (E + m_e)\left[(1 - \kappa^2)s, 0, 0, 0\right], \tag{7.4}$$

$$j_{e\uparrow\downarrow} = \bar{u}_\downarrow(p_3)\gamma^\mu u_\uparrow(p_1) = (E + m_e)\left[(\kappa^2 - 1)s, 0, 0, 0\right]. \tag{7.5}$$

Thus, in the relativistic limit where $\kappa \approx 1$, only two of the four helicity combinations give non-zero electron currents, reflecting the chiral nature of the QED interaction vertex. At lower energies, where $\kappa < 1$, all four helicity combinations give non-zero matrix elements; in this limit the helicity eigenstates no longer correspond to the chiral eigenstates and helicity is not conserved in the interaction.

In the limit where the velocity of the recoiling proton is small ($\beta_p \ll 1$), the lower two components of the corresponding particle spinors are approximately zero (since $\kappa \approx 0$). Taking the spherical polar angles defining the direction of the (relatively small) recoil momentum of the proton as ($\theta_p = \eta$, $\phi_p = \pi$), the initial-state and final-state protons can be described respectively by the helicity states

$$u_\uparrow(p_2) = \sqrt{2m_p}\begin{pmatrix}1\\0\\0\\0\end{pmatrix} \equiv u_1(p_2) \quad \text{and} \quad u_\downarrow(p_2) = \sqrt{2m_p}\begin{pmatrix}0\\1\\0\\0\end{pmatrix} \equiv u_2(p_2),$$

and

$$u_\uparrow(p_4) \approx \sqrt{2m_p}\begin{pmatrix}c_\eta\\-s_\eta\\0\\0\end{pmatrix} \quad \text{and} \quad u_\downarrow(p_4) \approx \sqrt{2m_p}\begin{pmatrix}-s_\eta\\-c_\eta\\0\\0\end{pmatrix},$$

where $c_\eta = \cos(\eta/2)$ and $s_\eta = \sin(\eta/2)$. The proton four-vector currents for the four possible combinations of the initial- and final-state helicity states, again calculated using (6.12)–(6.15), are

$$j_{p\uparrow\uparrow} = -j_{p\downarrow\downarrow} = 2m_p\left[c_\eta, 0, 0, 0\right] \quad \text{and} \quad j_{p\uparrow\downarrow} = j_{p\downarrow\uparrow} = -2m_p\left[s_\eta, 0, 0, 0\right]. \tag{7.6}$$

Thus, in the limit where the proton recoil momentum is small, all four spin combinations for the proton current contribute to the scattering process.

From the QED matrix element,

$$\mathcal{M}_{fi} = \frac{e^2}{q^2} j_e \cdot j_p,$$

and the expressions for the electron and proton currents of (7.2)–(7.6), the spin-averaged matrix element squared is

$$\begin{aligned}\langle|\mathcal{M}_{fi}^2|\rangle &= \frac{1}{4}\sum|\mathcal{M}_{fi}^2| \\ &= \frac{1}{4}\frac{e^4}{q^4}\times 4m_{\mathrm{p}}^2(E+m_{\mathrm{e}})^2\cdot\left[c_\eta^2+s_\eta^2\right]\cdot\left[4(1+\kappa^2)^2c^2+4(1-\kappa^2)^2s^2\right] \\ &= \frac{4m_{\mathrm{p}}^2m_{\mathrm{e}}^2e^4(\gamma_{\mathrm{e}}+1)^2}{q^4}\left[(1-\kappa^2)^2+4\kappa^2c^2\right], \end{aligned} \tag{7.7}$$

where in the last step, the electron energy was written as $E = \gamma_{\mathrm{e}}m_{\mathrm{e}}$. The above expression can be simplified further by writing

$$\kappa = \frac{\beta_{\mathrm{e}}\gamma_{\mathrm{e}}}{\gamma_{\mathrm{e}}+1} \quad \text{and} \quad (1-\beta_{\mathrm{e}}^2)\gamma_{\mathrm{e}}^2 = 1,$$

in which case, after some algebraic manipulation, (7.7) becomes

$$\langle|\mathcal{M}_{fi}^2|\rangle = \frac{16m_{\mathrm{p}}^2m_{\mathrm{e}}^2e^4}{q^4}\left[1+\beta_{\mathrm{e}}^2\gamma_{\mathrm{e}}^2\cos^2\frac{\theta}{2}\right]. \tag{7.8}$$

In the t-channel $\mathrm{e}^-\mathrm{p}\to\mathrm{e}^-\mathrm{p}$ scattering process, the square of four-momentum carried by the virtual photon is given by

$$q^2 = (p_1-p_3)^2.$$

For the elastic scattering process where the recoil of the proton can be neglected, the energies and momenta of the initial- and final-state electrons are $E_1 = E_3 = E$ and $\mathrm{p}_1 = \mathrm{p}_3 = \mathrm{p}$, and hence

$$q^2 = (0,\mathbf{p}_1-\mathbf{p}_3)^2 = -2\mathrm{p}^2(1-\cos\theta) = -4\mathrm{p}^2\sin^2(\theta/2).$$

Substituting this expression for q^2 into (7.8) gives

$$\langle|\mathcal{M}_{fi}^2|\rangle = \frac{m_{\mathrm{p}}^2m_{\mathrm{e}}^2e^4}{\mathrm{p}^4\sin^4(\theta/2)}\left[1+\beta_{\mathrm{e}}^2\gamma_{\mathrm{e}}^2\cos^2\frac{\theta}{2}\right]. \tag{7.9}$$

Provided the proton recoil can be neglected, this matrix element is equally applicable when the electron is either non-relativistic or relativistic.

7.2.1 Rutherford scattering

Rutherford scattering is the limit where the proton recoil can be neglected and the electron is non-relativistic, $\beta_{\mathrm{e}}\gamma_{\mathrm{e}} \ll 1$. In this case, the spin-averaged matrix element squared of (7.9) reduces to

$$\langle|\mathcal{M}_{fi}^2|\rangle = \frac{m_{\mathrm{p}}^2m_{\mathrm{e}}^2e^4}{\mathrm{p}^4\sin^4(\theta/2)}. \tag{7.10}$$

The laboratory frame differential cross section is obtained from the cross section formula of (3.48),

$$\frac{\mathrm{d}\sigma}{\mathrm{d}\Omega} = \frac{1}{64\pi^2}\left(\frac{1}{m_\mathrm{p} + E_1 - E_1\cos\theta}\right)^2 \langle|\mathcal{M}_{fi}|^2\rangle. \tag{7.11}$$

In the Rutherford scattering limit, where the electron is non-relativistic, $E_1 \sim m_\mathrm{e} \ll m_\mathrm{p}$, and (7.11) therefore reduces to

$$\frac{\mathrm{d}\sigma}{\mathrm{d}\Omega} = \frac{1}{64\pi^2 m_\mathrm{p}^2}\langle|\mathcal{M}_{fi}|^2\rangle = \frac{m_\mathrm{e}^2 e^4}{64\pi^2 \mathrm{p}^4 \sin^4(\theta/2)}\,. \tag{7.12}$$

Equation (7.12) can be expressed in the more usual form by writing the kinetic energy of the non-relativistic electron as $E_K = \mathrm{p}^2/2m_\mathrm{e}$ and writing $e^2 = 4\pi\alpha$ to give

$$\left(\frac{\mathrm{d}\sigma}{\mathrm{d}\Omega}\right)_\mathrm{Rutherford} = \frac{\alpha^2}{16E_K^2\sin^4(\theta/2)}. \tag{7.13}$$

The Rutherford scattering cross section of (7.13) is usually derived from first-order perturbation theory by considering the scattering of a non-relativistic electron in the *static* Coulomb potential of the proton, $V(\mathrm{r}) = \alpha/\mathrm{r}$. Therefore, it can be concluded that in the non-relativistic limit, only the interaction between the electric charges of the electron and proton contribute to the scattering process; there is no significant contribution from the magnetic (spin–spin) interaction. It should be noted that the angular dependence of the Rutherford scattering cross section originates solely from the $1/q^2$ propagator term.

7.2.2 Mott scattering

Mott scattering is the limit of electron–proton elastic scattering where the electron is relativistic but the proton recoil still can be neglected. These conditions apply when $m_\mathrm{e} \ll E \ll m_\mathrm{p}$. In this case, the parameter $\kappa \approx 1$ and two of the four possible electron currents of (7.2)–(7.5) are zero. Writing $E = \gamma_\mathrm{e} m_\mathrm{e}$ and taking the limit $\beta_\mathrm{e}\gamma_\mathrm{e} \gg 1$ for which $E \approx \mathrm{p}$, the matrix element of (7.9) reduces to

$$\langle|\mathcal{M}_{fi}^2|\rangle \approx \frac{m_\mathrm{p}^2 e^4}{E^2\sin^4(\theta/2)}\cos^2\frac{\theta}{2},$$

which when substituted into (7.11) gives

$$\left(\frac{\mathrm{d}\sigma}{\mathrm{d}\Omega}\right)_\mathrm{Mott} = \frac{\alpha^2}{4E^2\sin^4(\theta/2)}\cos^2\frac{\theta}{2}. \tag{7.14}$$

The Mott scattering cross section formula of (7.14) could have been derived by considering the scattering of a relativistic electron in the Coulomb potential of a

spin-less nucleus. Again it can be concluded that the contribution to the scattering process from a purely magnetic spin–spin interaction is negligible.

7.3 Form factors

The Rutherford and Mott scattering formulae of (7.13) and (7.14) can be calculated from first-order perturbation theory for scattering in the Coulomb potential from a *point-like object*. To account for the finite extent of the charge distribution of the proton, this treatment must be modified by introducing a *form factor*. Qualitatively, the form factor accounts for the phase differences between contributions to the scattered wave from different points of the charge distribution, as indicated in Figure 7.3. If the wavelength of the virtual photon is much larger than the radius of the proton, the contributions to the scattered wave from each point in the charge distribution will be in phase and therefore add constructively. When the wavelength is smaller than the radius of the proton, the phases of the scattered waves will have a strong dependence on the position of the part of the charge distribution responsible for the scattering. In this case, when integrated over the entire charge distribution, the negative interference between the different contributions greatly reduces the total amplitude.

The mathematical expression for the form factor (which is not a Lorentz-invariant concept) can be derived in the context of first-order perturbation theory. Consider the scattering of an electron in the static potential from an extended charge distribution, as indicated in Figure 7.4. The charge density can be written as $Q\rho(\mathbf{r}')$,

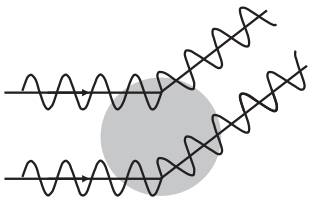

Fig. 7.3 A cartoon indicating the origin of the form factor in elastic scattering.

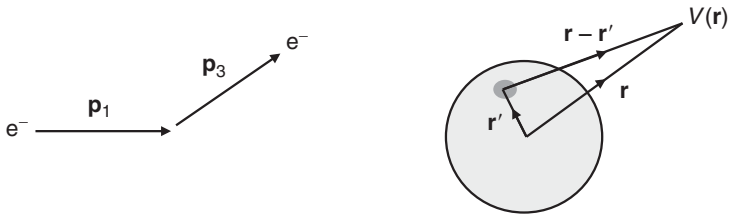

Fig. 7.4 The potential due to an extended charge distribution.

where Q is the total charge and $\rho(\mathbf{r}')$ is the charge distribution normalised to unity

$$\int \rho(\mathbf{r}')\,\mathrm{d}^3\mathbf{r}' = 1\,.$$

The potential at a distance $\mathbf{r}$ from the origin, written in terms of this charge density is simply

$$V(\mathbf{r}) = \int \frac{Q\rho(\mathbf{r}')}{4\pi|\mathbf{r}-\mathbf{r}'|}\mathrm{d}^3\mathbf{r}'\,. \tag{7.15}$$

In the Born approximation, where the wavefunctions of the initial-state and scattered electrons are expressed as the plane waves, $\psi_i = e^{i(\mathbf{p}_1\cdot\mathbf{r}-Et)}$ and $\psi_f = e^{i(\mathbf{p}_3\cdot\mathbf{r}-Et)}$, the lowest-order matrix element for the scattering process is

$$\mathcal{M}_{fi} = \langle\psi_f|V(\mathbf{r})|\psi_i\rangle = \int e^{-i\mathbf{p}_3\cdot\mathbf{r}}V(\mathbf{r})e^{i\mathbf{p}_1\cdot\mathbf{r}}\,\mathrm{d}^3\mathbf{r}.$$

Writing $\mathbf{q} = (\mathbf{p}_1 - \mathbf{p}_3)$ and using the potential of (7.15) leads to

$$\begin{aligned}\mathcal{M}_{fi} &= \iint e^{i\mathbf{q}\cdot\mathbf{r}}\frac{Q\rho(\mathbf{r}')}{4\pi|\mathbf{r}-\mathbf{r}'|}\,\mathrm{d}^3\mathbf{r}'\mathrm{d}^3\mathbf{r}\\ &= \iint e^{i\mathbf{q}\cdot(\mathbf{r}-\mathbf{r}')}e^{i\mathbf{q}\cdot\mathbf{r}'}\frac{Q\rho(\mathbf{r}')}{4\pi|\mathbf{r}-\mathbf{r}'|}\,\mathrm{d}^3\mathbf{r}'\mathrm{d}^3\mathbf{r}\,.\end{aligned} \tag{7.16}$$

By expressing the difference $\mathbf{r}-\mathbf{r}'$ as the vector $\mathbf{R}$, the integral of (7.16) separates into two parts

$$\mathcal{M}_{fi} = \int e^{i\mathbf{q}\cdot\mathbf{R}}\frac{Q}{4\pi|\mathbf{R}|}\mathrm{d}^3\mathbf{R}\int\rho(\mathbf{r}')e^{i\mathbf{q}\cdot\mathbf{r}'}\,\mathrm{d}^3\mathbf{r}'\,.$$

The integral over $\mathrm{d}^3\mathbf{R}$ is simply the equivalent expression for scattering from a potential due to a point charge. Hence the matrix element can be written

$$\mathcal{M}_{fi} = \mathcal{M}^{\mathrm{pt}}_{fi}F(\mathbf{q}^2),$$

where $\mathcal{M}^{\mathrm{pt}}_{fi}$ is the equivalent matrix element for a point-like proton and the form factor $F(\mathbf{q}^2)$ is given by

$$F(\mathbf{q}^2) = \int\rho(\mathbf{r})e^{i\mathbf{q}\cdot\mathbf{r}}\,\mathrm{d}^3\mathbf{r}.$$

Therefore, in order to account for the extended charge distribution of the proton, the Mott scattering cross section of (7.14) has to be modified to

$$\left(\frac{\mathrm{d}\sigma}{\mathrm{d}\Omega}\right)_{\mathrm{Mott}} \to \frac{\alpha^2}{4E^2\sin^4(\theta/2)}\cos^2\left(\frac{\theta}{2}\right)\left|F(\mathbf{q}^2)\right|^2\,. \tag{7.17}$$

The form factor $F(\mathbf{q}^2)$ is the three-dimensional Fourier transform of the charge distribution. If the wavelength of the virtual photon is large compared to the size of

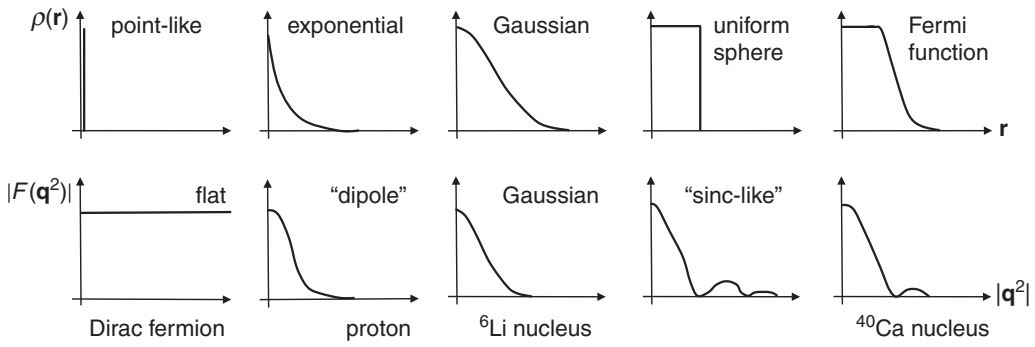

Fig. 7.5 Possible three-dimensional charge distributions and the corresponding form factors plotted as a function of $\mathbf{q}^2$.

the charge distribution then $\mathbf{q} \cdot \mathbf{r} \approx 0$ over the entire volume integral. In this case, the scattering cross section is identical to that for a point-like object and therefore, regardless of the form of the charge distribution, $F(0) = 1$. In the limit where the wavelength is very small compared with the size of the charge distribution, the phases of the contributions from different regions of the charge distribution will vary rapidly and will tend to cancel and $F(\mathbf{q}^2 \to \infty) = 0$. Thus, for *any* finite size charge distribution, the elastic scattering cross section will tend to zero at high values of $\mathbf{q}^2$. The exact form of $F(\mathbf{q}^2)$ depends on the charge distribution; some common examples and the corresponding form factors are shown in Figure 7.5. For a point-like particle, $F(\mathbf{q}^2) = 1$ for all $\mathbf{q}$.

7.4 Relativistic electron–proton elastic scattering

In the above calculations of the Rutherford and Mott elastic scattering cross sections, it was assumed that the recoil of the proton could neglected. This a reasonable approximation provided $|\mathbf{q}| \ll m_\mathrm{p}$. In this low-energy limit, it was inferred that the contribution to the scattering process from the pure magnetic spin–spin interaction is negligibly small. For electron–proton elastic scattering at higher energies, the recoil of the proton cannot be neglected and the magnetic spin–spin interaction becomes important.

For the general case, the four-momenta of the initial- and final-state particles, defined in Figure 7.6, can be written as

$$p_1 = (E_1, 0, 0, E_1), \tag{7.18}$$
$$p_2 = (m_\mathrm{p}, 0, 0, 0), \tag{7.19}$$
$$p_3 = (E_3, 0, E_3 \sin\theta, E_3 \cos\theta), \tag{7.20}$$
$$p_4 = (E_4, \mathbf{p}_4). \tag{7.21}$$

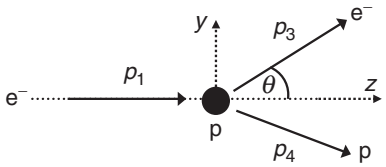

Fig. 7.6 The kinematics of electron–proton scattering in the proton rest frame.

Here the energy of the scattered electron is no longer equal to that of the incident electron. Assuming that the electron energy is sufficiently large that terms of $O(m_e^2)$ can be neglected, and (initially) treating the proton as a point-like Dirac particle, the matrix element for the elastic scattering process $e^-p \to e^-p$ is given by (6.67)

$$\langle|\mathcal{M}_{fi}|^2\rangle = \frac{8e^4}{(p_1 - p_3)^4}\left[(p_1.p_2)(p_3.p_4) + (p_1.p_4)(p_2.p_3) - m_p^2(p_1.p_3)\right]. \quad (7.22)$$

7.4.1 Scattering kinematics

In most electron–proton elastic scattering experiments, the final-state proton is not observed. Consequently, the matrix element of (7.22) is most usefully expressed in terms of the experimental observables, which are the energy and scattering angle of the electron. To achieve this, the final-state proton four-momentum p_4 can be eliminated using energy and momentum conservation, $p_4 = p_1 + p_2 - p_3$. From the definitions of the four-momenta in (7.18)–(7.20), the four-vector scalar products in (7.22) which do not involve p_4 are

$$p_2\cdot p_3 = E_3 m_p, \quad p_1\cdot p_2 = E_1 m_p \quad \text{and} \quad p_1\cdot p_3 = E_1E_3(1-\cos\theta).$$

The two terms involving p_4, which can be rewritten using $p_4 = p_1 + p_2 - p_3$, are

$$p_3\cdot p_4 = p_3\cdot p_1 + p_3\cdot p_2 - p_3\cdot p_3 = E_1E_3(1-\cos\theta) + E_3m_p,$$
$$p_1\cdot p_4 = p_1\cdot p_1 + p_1\cdot p_2 - p_1\cdot p_3 = E_1m_p - E_1E_3(1-\cos\theta),$$

where the terms $p_1\cdot p_1 = p_3\cdot p_3 = m_e^2$ have been been dropped. Hence, the matrix element of (7.22), expressed in terms of the energy of the final-state electron E_3 and the scattering angle θ is

$$\begin{aligned}\langle|\mathcal{M}_{fi}|^2\rangle &= \frac{8e^4}{(p_1-p_3)^4}m_pE_1E_3\left[(E_1-E_3)(1-\cos\theta) + m_p[(1+\cos\theta)\right] \\ &= \frac{8e^4}{(p_1-p_3)^4}2m_pE_1E_3\left[(E_1-E_3)\sin^2\frac{\theta}{2} + m_p\cos^2\frac{\theta}{2}\right]. \end{aligned} \quad (7.23)$$

The four-momentum squared of the virtual photon, $q^2 = (p_1 - p_3)^2$, also can be expressed in terms of E_3 and θ using

$$q^2 = (p_1-p_3)^2 = p_1^2 + p_3^2 - 2p_1\cdot p_3 \approx -2E_1E_3(1-\cos\theta), \quad (7.24)$$

where again the terms $p_1 \cdot p_1 = p_3 \cdot p_3 = m_e^2$ have been neglected. Hence, to a good approximation,

$$q^2 = -4E_1 E_3 \sin^2 \frac{\theta}{2}. \tag{7.25}$$

Because q^2 is always negative, it is more convenient to work in terms of Q^2 defined by

$$Q^2 \equiv -q^2 = 4E_1 E_3 \sin^2 \frac{\theta}{2}, \tag{7.26}$$

which is always positive.

The energy lost by the electron in the scattering process, $E_1 - E_3$, can be expressed in terms of Q^2 by first noting that

$$q \cdot p_2 = (p_1 - p_3) \cdot p_2 = m_p (E_1 - E_3). \tag{7.27}$$

A second equation for $q \cdot p_2$ can be obtained by expressing q in terms of the proton four-momenta, $q = p_4 - p_2$, such that

$$p_4^2 = (q + p_2)^2 = q^2 + 2q \cdot p_2 + p_2^2,$$

which, using $p_2^2 = p_4^2 = m_p^2$, gives

$$q \cdot p_2 = -q^2/2. \tag{7.28}$$

Equating (7.27) and (7.28) enables $(E_1 - E_3)$ to be expressed as a function of Q^2,

$$E_1 - E_3 = -\frac{q^2}{2m_p} = \frac{Q^2}{2m_p}, \tag{7.29}$$

which (unsurprisingly) demonstrates that the electron always loses energy in the scattering process. Using the relations of (7.25) and (7.29), the spin-averaged matrix element squared of (7.23) can be expressed as

$$\langle |\mathcal{M}_{fi}|^2 \rangle = \frac{m_p^2 e^4}{E_1 E_3 \sin^4(\theta/2)} \left[\cos^2 \frac{\theta}{2} + \frac{Q^2}{2m_p^2} \sin^2 \frac{\theta}{2} \right].$$

The differential cross section again can be obtained the cross section formula of (3.47), giving

$$\frac{\mathrm{d}\sigma}{\mathrm{d}\Omega} \approx \frac{1}{64\pi^2} \left(\frac{E_3}{m_p E_1} \right)^2 \langle |\mathcal{M}_{fi}|^2 \rangle.$$

Hence, the differential cross section for the scattering of relativistic electrons from a proton that is initially at rest is

$$\frac{\mathrm{d}\sigma}{\mathrm{d}\Omega} = \frac{\alpha^2}{4E_1^2 \sin^4(\theta/2)} \frac{E_3}{E_1} \left(\cos^2 \frac{\theta}{2} + \frac{Q^2}{2m_p^2} \sin^2 \frac{\theta}{2} \right). \tag{7.30}$$

Although (7.30) is expressed in terms of Q^2, E_3 and θ, it is important to realise that there is only one independent variable; both Q^2 and E_3 can be expressed in terms of the scattering angle of the electron. This can be seen by firstly equating (7.24) and (7.29) to give

$$-2m_{\mathrm{p}}(E_1 - E_3) = -2E_1E_3(1 - \cos\theta),$$

and hence

$$E_3 = \frac{E_1 m_{\mathrm{p}}}{m_{\mathrm{p}} + E_1(1 - \cos\theta)}. \tag{7.31}$$

Substituting (7.31) back into (7.24) then gives an expression for Q^2 in terms of the electron scattering angle

$$Q^2 = \frac{2m_{\mathrm{p}}E_1^2(1 - \cos\theta)}{m_{\mathrm{p}} + E_1(1 - \cos\theta)}. \tag{7.32}$$

Therefore, if the scattering angle of the electron is measured in the elastic scattering process, the entire kinematics of the interaction are determined. In practice, measuring the $e^-p \to e^-p$ differential cross section boils down to counting the number of electrons scattered in a particular direction for a known incident electron flux. Furthermore, because the energy of an elastically scattered electron at a particular angle must be equal to that given by (7.31), by measuring the energy *and* angle of the scattered electron, it is possible to confirm that the interaction was indeed elastic and that the *unobserved* proton remained intact.

In the limit of $Q^2 \ll m_{\mathrm{p}}^2$ and $E_3 \approx E_1$, the expression for the electron–proton differential cross section of (7.30) reduces to that for Mott scattering, demonstrating that the Mott scattering cross section formula applies when $m_{\mathrm{e}} \ll E_1 \ll m_{\mathrm{p}}$. Equation (7.30) differs from the Mott scattering formula by the additional factor E_3/E_1, which accounts for the energy lost by electron due the proton recoil, and by the new term proportional to $\sin^2(\theta/2)$, which can be identified as being due to a purely magnetic spin–spin interaction.

7.5 The Rosenbluth formula

Equation (7.30) is the differential cross section for elastic $e^-p \to e^-p$ scattering assuming a point-like spin-half proton. The finite size of the proton is accounted for by introducing two form factors, one related to the charge distribution of the proton, $G_E(Q^2)$, and the other related to the magnetic moment distribution within the proton, $G_M(Q^2)$. It can be shown that the most general Lorenz-invariant form

for electron–proton scattering via the exchange of a single photon, known as the *Rosenbluth formula*, is

$$\frac{\mathrm{d}\sigma}{\mathrm{d}\Omega} = \frac{\alpha^2}{4E_1^2 \sin^4(\theta/2)} \frac{E_3}{E_1} \left(\frac{G_E^2 + \tau G_M^2}{(1+\tau)} \cos^2 \frac{\theta}{2} + 2\tau G_M^2 \sin^2 \frac{\theta}{2} \right), \tag{7.33}$$

where τ is given by

$$\tau = \frac{Q^2}{4m_\mathrm{p}^2}. \tag{7.34}$$

In the Lorentz-invariant Rosenbluth formula, the form factors $G_E(Q^2)$ and $G_M(Q^2)$ are functions of the four-momentum squared of the virtual photon. Unlike the form factor $F(\mathbf{q}^2)$ introduced previously, which was a function of the three-momentum squared, the form factors $G_E(Q^2)$ and $G_M(Q^2)$ cannot be interpreted simply as the Fourier transforms of the charge and magnetic moment distributions of the proton. However, the relation between $G_E(Q^2)$ and $G_M(Q^2)$ and the corresponding Fourier transforms can be obtained by writing

$$Q^2 = -q^2 = \mathbf{q}^2 - (E_1 - E_3)^2,$$

which from (7.29) gives

$$Q^2 \left(1 + \frac{Q^2}{4m_\mathrm{p}^2} \right) = \mathbf{q}^2 .$$

Therefore, in the limit where $Q^2 \ll 4m_\mathrm{p}^2$, the time-like component of Q^2 is relatively small and $Q^2 \approx \mathbf{q}^2$. Thus, in this low-Q^2 limit, the form factors $G_E(Q^2)$ and $G_M(Q^2)$ approximate to functions of $\mathbf{q}^2$ alone and can be interpreted as the Fourier transforms of the charge and magnetic moment distributions of the proton

$$G_E(Q^2) \approx G_E(\mathbf{q}^2) = \int e^{i\mathbf{q}\cdot\mathbf{r}} \rho(\mathbf{r}) \mathrm{d}^3\mathbf{r},$$

$$G_M(Q^2) \approx G_M(\mathbf{q}^2) = \int e^{i\mathbf{q}\cdot\mathbf{r}} \mu(\mathbf{r}) \mathrm{d}^3\mathbf{r} .$$

There is one further complication. The form of the Rosenbluth equation follows from (7.30), which was obtained from the QED calculation where the proton was treated as a point-like Dirac particle. But the magnetic moment of a point-like Dirac particle (see Appendix B.1) is related to its spin by

$$\boldsymbol{\mu} = \frac{q}{m}\mathbf{S},$$

whereas the experimentally measured value of the *anomalous* magnetic moment of the proton (discussed further in Chapter 9) is

$$\boldsymbol{\mu} = 2.79 \frac{e}{m_\mathrm{p}} \mathbf{S} .$$

For consistency with this experimental observation, the magnetic moment distribution has to be normalised to +2.79 rather than unity, and therefore

$$G_E(0) = \int \rho(\mathbf{r})\, \mathrm{d}^3\mathbf{r} = 1$$
$$G_M(0) = \int \mu(\mathbf{r})\, \mathrm{d}^3\mathbf{r} = +2.79.$$

It is worth noting that, even taken in isolation, the observation of the anomalous magnetic moment of the proton already provides evidence that the proton is not a point-like particle.

7.5.1 Measuring $G_E(Q^2)$ and $G_M(Q^2)$

The $e^- p \rightarrow e^- p$ differential cross section is a function of both the charge and magnetic moment distributions of the proton. Whilst it is tempting to assume that magnetic moment distribution follows that of the charge distribution, $G_M(Q^2) = 2.79\, G_E(Q^2)$, there is no *a priori* justification for making this assumption. Fortunately $G_M(Q^2)$ and $G_E(Q^2)$ can be determined separately from experiment. This can be seen by writing the Rosenbluth formula of (7.33) as

$$\frac{\mathrm{d}\sigma}{\mathrm{d}\Omega} = \left(\frac{G_E^2 + \tau G_M^2}{(1+\tau)} + 2\tau G_M^2 \tan^2 \frac{\theta}{2} \right) \cdot \left(\frac{\mathrm{d}\sigma}{\mathrm{d}\Omega} \right)_0, \tag{7.35}$$

where

$$\left(\frac{\mathrm{d}\sigma}{\mathrm{d}\Omega} \right)_0 = \frac{\alpha^2}{4E_1^2 \sin^4(\theta/2)} \left(\frac{E_3}{E_1} \right) \cos^2 \frac{\theta}{2}, \tag{7.36}$$

is the Mott cross section, modified to account for the proton recoil. At low Q^2, where $\tau \ll 1$, the electric form factor dominates and (7.35) is approximately

$$\frac{\mathrm{d}\sigma}{\mathrm{d}\Omega} \Big/ \left(\frac{\mathrm{d}\sigma}{\mathrm{d}\Omega} \right)_0 \approx G_E^2.$$

In this limit, G_E^2 is equivalent to the form factor $|F(\mathbf{q})|^2$ described previously. At high Q^2, where $\tau \gg 1$, the purely magnetic spin–spin term dominates and (7.35) approximates to

$$\frac{\mathrm{d}\sigma}{\mathrm{d}\Omega} \Big/ \left(\frac{\mathrm{d}\sigma}{\mathrm{d}\Omega} \right)_0 \approx \left(1 + 2\tau \tan^2 \frac{\theta}{2} \right) G_M^2.$$

In general, the Q^2 dependence of $G_M(Q^2)$ and $G_E(Q^2)$ can be inferred from $e^- p \rightarrow e^- p$ elastic scattering experiments by varying the electron beam energy. For each beam energy, the differential cross section is measured at the angle corresponding to a particular value of Q^2, given by (7.32). For example, Figure 7.7a

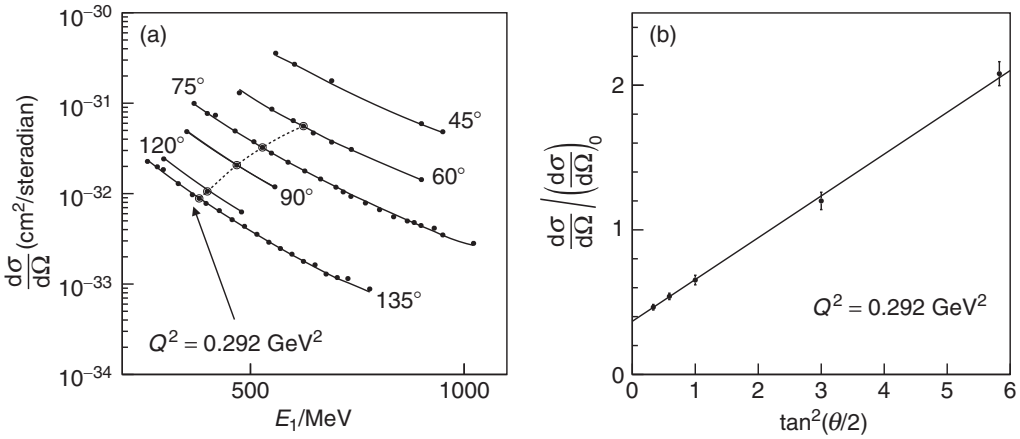

Fig. 7.7 Low energy $e^-p \to e^-p$ elastic scattering data. Data from Hughes *et al.* (1965).

shows the measured $e^-p \to e^-p$ differential cross sections for six different scattering angles and a range of beam energies. The five data points that are highlighted all correspond to $e^-p \to e^-p$ elastic scattering at $Q^2 = 0.292\,\text{GeV}^2$. In this way, the cross section can be measured at fixed Q^2 but over a range of scattering angles. Figure 7.7b shows, for the five data points with $Q^2 = 0.292\,\text{GeV}^2$, the measured cross sections normalised to the expected Mott cross section of (7.36), plotted as a function of $\tan^2(\theta/2)$. The observed linear dependence on $\tan^2(\theta/2)$ is expected from (7.35), where it can be seen that the gradient and intercept with the y-axis are given respectively by

$$m = 2\tau \left[G_M(Q^2)\right]^2 \quad \text{and} \quad c = \frac{\left[G_E(Q^2)\right]^2 + \tau \left[G_M(Q^2)\right]^2}{(1+\tau)}.$$

Hence, the data shown in Figure 7.7b can be used to extract measurements of both $G_E(Q^2)$ and $G_M(Q^2)$ at $Q^2 = 0.292\,\text{GeV}^2$ (see Problem 7.6). A similar analysis can be applied to cross section measurements corresponding to different values of Q^2, providing an experimental determination of the electric and magnetic form factors of the proton over a range of Q^2 values, as shown in Figure 7.8a. The fact that the measured form factors decrease with Q^2 provides a concrete experimental demonstration that the proton has finite size. The shape of $G_M(Q^2)$ closely follows that of $G_E(Q^2)$, showing that the charge and magnetic moment distributions within the proton are consistent. Furthermore, the measured values extrapolated to $Q^2 = 0$ are in agreement with the expectations of $G_E(0) = 1$ and $G_M(0) = 2.79$. Finally, Figure 7.8b shows measurements of $G_M(Q^2)$ at Q^2 values up to $32\,\text{GeV}^2$. For these data recorded at higher values of Q^2, the contribution from $G_E(Q^2)$ is strongly suppressed and only $G_M(Q^2)$ can be measured.

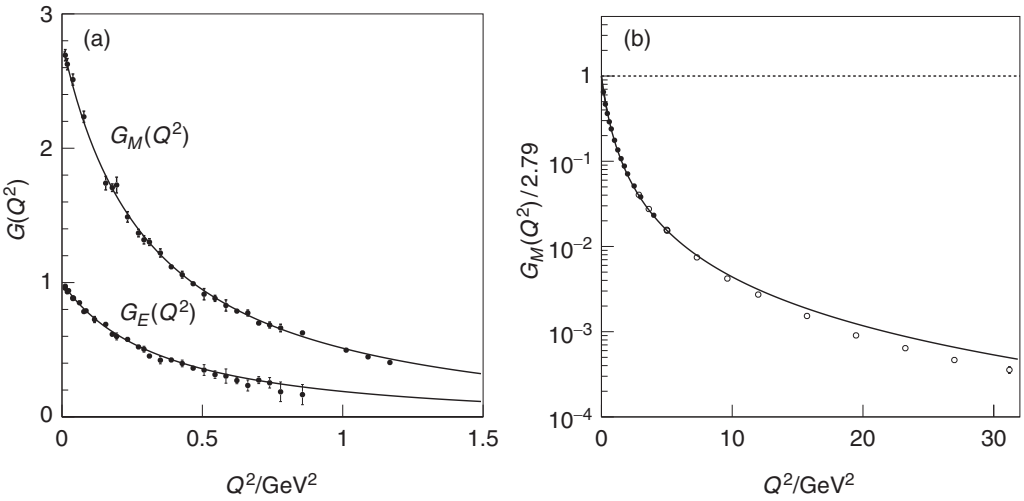

Fig. 7.8 (a) Measurements of $G_E(Q^2)$ and $G_M(Q^2)$ from $e^- p \rightarrow e^- p$ elastic scattering data at low Q^2, adapted from Hughes *et al.* (1965) and references therein. (b) Measurements of $G_M(Q^2)$ at higher Q^2, data from Walker *et al.* (1994) (solid circles) and Sill *et al.* (1993) (open circles). The curves correspond to the dipole function described in the text.

The data shown in Figures 7.8a and 7.8b are reasonably well parameterised by the empirically determined "dipole function"

$$G_M(Q^2) = 2.79 G_E(Q^2) \approx 2.79 \frac{1}{(1 + Q^2/0.71\,\mathrm{GeV}^2)^2}. \tag{7.37}$$

By taking the Fourier transform of the dipole function for $G_E(Q^2)$, which provides a good description of the low Q^2 data where $Q^2 \approx \mathbf{q}^2$, the charge distribution of the proton is determined to be

$$\rho(\mathbf{r}) \approx \rho_0 e^{-\mathrm{r}/a},$$

with $a \approx 0.24$ fm. This experimentally determined value for a corresponds to a proton root-mean-square charge radius of 0.8 fm.

7.5.2 Elastic scattering at high Q^2

At high Q^2, the electron–proton elastic scattering cross section of (7.35) reduces to

$$\left(\frac{\mathrm{d}\sigma}{\mathrm{d}\Omega}\right)_{\text{elastic}} \sim \frac{\alpha^2}{4E_1^2 \sin^4(\theta/2)} \frac{E_3}{E_1} \left[\frac{Q^2}{2m_\mathrm{p}^2} G_M^2 \sin^2\frac{\theta}{2}\right].$$

From (7.37) it can be seen that in the high-Q^2 limit, $G_M(Q^2) \propto Q^{-4}$ and therefore

$$\left(\frac{\mathrm{d}\sigma}{\mathrm{d}\Omega}\right)_{elastic} \propto \frac{1}{Q^6} \left(\frac{\mathrm{d}\sigma}{\mathrm{d}\Omega}\right)_{Mott}.$$

Consequently, due to the finite size of the proton, the elastic scattering process becomes increasingly unlikely for interactions where the virtual photon has large Q^2. If the inelastic scattering process, where the proton breaks up, also involved a coherent interaction of the virtual photon with the charge and magnetic moment distribution of the proton as a whole, a similar high-Q^2 suppression of the cross section would be expected. In practice, no such suppression of the inelastic e^-p cross section is observed. This implies that the interaction takes place with the constituent parts of the proton rather than the proton as a whole. This process of high-energy deep inelastic scattering is the main topic of next chapter.

Summary

In this chapter, the process of $e^-p \rightarrow e^-p$ elastic scattering has been described in some detail. In general, the differential elastic scattering cross section is given by the Rosenbluth formula

$$\frac{d\sigma}{d\Omega} = \frac{\alpha^2}{4E_1^2 \sin^4(\theta/2)} \frac{E_3}{E_1} \left(\frac{G_E^2 + \tau G_M^2}{(1+\tau)} \cos^2 \frac{\theta}{2} + 2\tau G_M^2 \sin^2 \frac{\theta}{2} \right),$$

where the form factors $G_E(Q^2)$ and $G_M(Q^2)$ describe the charge and magnetic moment distributions of the proton. The techniques used to measure the form factors were described in some detail. It is important that you understand the concepts; they will be used again in the following chapter.

Because of the finite size of the proton, both $G_E(Q^2)$ and $G_M(Q^2)$ become small at high Q^2 and the elastic scattering cross section falls rapidly with increasing Q^2. Consequently, high-energy electron–proton scattering is dominated by inelastic processes where the virtual photon interacts with the quarks inside the proton, rather than the proton as a coherent whole.

Problems

7.1 The derivation of (7.8) used the algebraic relation

$$(\gamma+1)^2(1-\kappa^2)^2 = 4,$$

where

$$\kappa = \frac{\beta\gamma}{\gamma+1} \quad \text{and} \quad (1-\beta^2)\gamma^2 = 1.$$

Show that this holds.